

Learning Characteristics of Reverse Quaternion Neural Network ^{*}

Shogo Yamauchi¹[0009-0000-9011-4201], Tohru Nitta²[0000-0001-9628-7920], and Takaaki Ohnishi³[0009-0002-5732-0892]

¹ Asahi Shinbun Company, Tokyo, Japan
yamauchi-s1@asahi.com

² Tokyo Woman's Christian University, Tokyo, Japan
tnitta@lab.twcu.ac.jp

³ Rikkyo University, Tokyo, Japan
ohnishi@rikkyo.ac.jp

Abstract. The purpose of this paper is to propose a new multi-layer feedforward quaternion neural network model architecture, Reverse Quaternion Neural Network which utilizes the non-commutative nature of quaternion products, and to clarify its learning characteristics. While quaternion neural networks have been used in various fields, there has been no research report on the characteristics of multi-layer feedforward quaternion neural networks where weights are applied in the reverse direction. This paper investigates the learning characteristics of the Reverse Quaternion Neural Network from two perspectives: the learning speed and the generalization on rotation. As a result, it is found that the Reverse Quaternion Neural Network has a learning speed comparable to existing models and can obtain a different rotation representation from the existing models.

Keywords: neural network · learning · quaternion · non-commutative property · rotation

1 Introduction

In recent years, machine learning technology has made tremendous progress with the rise of deep learning. In particular, it has achieved remarkable success in fields such as image recognition, natural language processing, and speech recognition, and is still being actively researched. A high-dimensional neural network [1–5] is a type of neural network that uses numbers of two or more dimensions, such as complex numbers and quaternions, to represent the parameters of the neural network. High-dimensional neural networks can deal with hypercomplex-valued signals naturally. It is well-known that complex-valued neural networks and quaternion neural networks require fewer parameters (weights, biases) and

^{*} Part of this work has been done while the first author, Yamauchi, was a graduate student at Rikkyo University.

have several times faster learning speeds than usual real-valued neural networks [6–9].

Recent studies have actively explored the application of high-dimensional neural networks in areas such as speech recognition and image processing. Zhu et al. [10] have extended the convolutional neural networks (CNN) [11] to quaternions. This approach represents the relationship between RGB colors in an image through the rotation of quaternions in the imaginary parts (i , j , and k axes), and has shown higher accuracy in color image processing compared to real-valued convolutional neural networks. The quaternion convolutional neural network, proposed by Parcollet et al. [12], introduces a model that divides the feature map into individual components of quaternions and convolves them. This approach has demonstrated superior recognition capabilities in speech recognition tasks compared to real-valued CNNs.

A quaternion is a mathematical concept introduced by Hamilton [13] in 1843. A quaternion consists of a real part and three imaginary parts (i , j , k), each representing an independent dimension. This characteristic makes quaternions particularly suitable for representing rotations in a three-dimensional space. Furthermore, quaternions possess the property that the commutative law of multiplication does not apply, meaning that the order of multiplication significantly affects the outcome. As described below, neural networks utilizing quaternions exhibit different characteristics compared to real-valued and complex-valued neural networks in this meaning.

A quaternion neural network is a neural network model where all parameters are represented as quaternions, enabling the network using quaternions to represent data in higher dimensions, and it particularly excels in representing rotations and orientations in three-dimensional space. By utilizing the rich expressiveness of quaternions, quaternion neural networks can capture spatial data features that traditional neural networks may miss, especially in fields where spatial information is crucial, such as 3D graphics and robotics.

In the context of 3D spatial transformations, Matsui et al. [14] conducted an experiment comparing three tasks - scaling, parallel translation, and rotation - using geometric object data with the Quaternion Multi-layer Perceptron (QMLP) and the real-valued MLP (Multi-layer Perceptron). The results showed that while the real-valued MLP failed to learn the transformations, the QMLP successfully learned them and performed perfectly in all three tasks.

The existence of two types of quaternion neurons, based on non-commutativity, was pointed out in [7]. Yoshida et al. [15] investigated the existence conditions of the energy functions for the Hopfield-type recurrent quaternion neural network and the one with weights applied in reverse order. As a result, they clarified that there is no difference between the usual Hopfield-type recurrent quaternion neural network model and the quaternion neural network with weights applied in reverse order.

In this paper, we propose a new feedforward quaternion neural network architecture, Reverse Quaternion Neural Networks (called RQNN for short here), which utilizes the non-commutative property of quaternions. In the model, by

altering the order of quaternion multiplication, it is possible to construct neural networks with different characteristics. This approach is expected to capture information and offer a different expressive power that traditional quaternion neural networks cannot achieve. As a matter of facts , we conducted experiments on the learning speed and the generalization ability on rotation of the RQNN and the usual multi-layer feedforward quaternion neural network, and showed the differences between the two quaternion neural networks.

2 Reverse Quaternion Neural Network Architecture

In this section, we formulate the RQNN architecture, and derive the learning algorithm.

2.1 Quaternion and Its Properties

First, we describe the quaternion and its properties.

The quaternion $q \in \mathbb{H}$ is defined as

$$q = a + bi + cj + dk \in \mathbb{H} \quad (a, b, c, d \in \mathbb{R}), \quad (1)$$

where a is the real part, b, c, d are the imaginary parts, \mathbb{H} is the set of quaternions, and \mathbb{R} is the set of real numbers. i, j, k are independent imaginary units, and the following arithmetic rules apply.

$$i^2 = j^2 = k^2 = ijk = -1. \quad (2)$$

$$ij = -ji = k, \quad ki = -ik = j, \quad jk = -kj = i. \quad (3)$$

For the two quaternions $q_1 = a_1 + b_1i + c_1j + d_1k \in \mathbb{H}$ and $q_2 = a_2 + b_2i + c_2j + d_2k \in \mathbb{H}$, their multiplication is calculated as follows:

$$\begin{aligned} q_1q_2 &= (a_1a_2 - b_1b_2 - c_1c_2 - d_1d_2) \\ &\quad + (a_1b_2 + b_1a_2 + c_1d_2 - d_1c_2) i \\ &\quad + (a_1c_2 - b_1d_2 + c_1a_2 + d_1b_2) j \\ &\quad + (a_1d_2 + b_1c_2 - c_1b_2 + d_1a_2) k. \end{aligned} \quad (4)$$

The reverse multiplication q_2q_1 is calculated as

$$\begin{aligned} q_2q_1 &= (a_2a_1 - b_2b_1 - c_2c_1 - d_2d_1) \\ &\quad + (a_2b_1 + b_2a_1 + c_2d_1 - d_2c_1) i \\ &\quad + (a_2c_1 - b_2d_1 + c_2a_1 + d_2b_1) j \\ &\quad + (a_2d_1 + b_2c_1 - c_2b_1 + d_2a_1) k. \end{aligned} \quad (5)$$

From Eqs. (4) and (5), it is evident that the multiplication of quaternions is *non-commutative*. The conjugate quaternion of $q = a + bi + cj + dk$, denoted as \bar{q} , is defined as

$$\bar{q} = a - bi - cj - dk. \quad (6)$$

2.2 A Reverse Quaternion Neuron

A neuron used in the RQNN is as follows. We call it a *reverse quaternion neuron*. The input signals, weights, biases, and output signals are all quaternions. The net input U_n to neuron n is defined to be

$$U_n = \sum_m W_{nm} S_m + T_n \in \mathbb{H}, \quad (7)$$

where $S_m \in \mathbb{H}$ is the quaternion input signal coming from the output of neuron m , $W_{nm} \in \mathbb{H}$ is the quaternion weight connecting neurons m and n , and $T_n \in \mathbb{H}$ is the quaternion bias of neuron n . Note here that the order of multiplication of a weight and an input signal is *WEIGHT times INPUT SIGNAL* (Eq. (7), Fig. 1). In a usual quaternion neuron, the order of multiplication of a weight and an input signal is *INPUT SIGNAL times WEIGHT* [5,7]. This is why it is called a reverse quaternion neuron. To obtain the quaternion output signal, convert the net input U_n into its four parts as follows.

$$U_n = u_1 + u_2i + u_3j + u_4k \in \mathbb{H}. \quad (8)$$

Although the activation function of a quaternion neuron is a quaternion function generally, we use the following activation function, known as *split-type*:

$$f(x) = f_R(x_1) + f_R(x_2)i + f_R(x_3)j + f_R(x_4)k \quad (9)$$

where $x = x_1 + x_2i + x_3j + x_4k \in \mathbb{H}$ and $f_R(x) : \mathbb{R} \rightarrow \mathbb{R}$ is a real-valued activation function applied to each component. Therefore, the output value of the neuron n is given by $f(U_n)$.

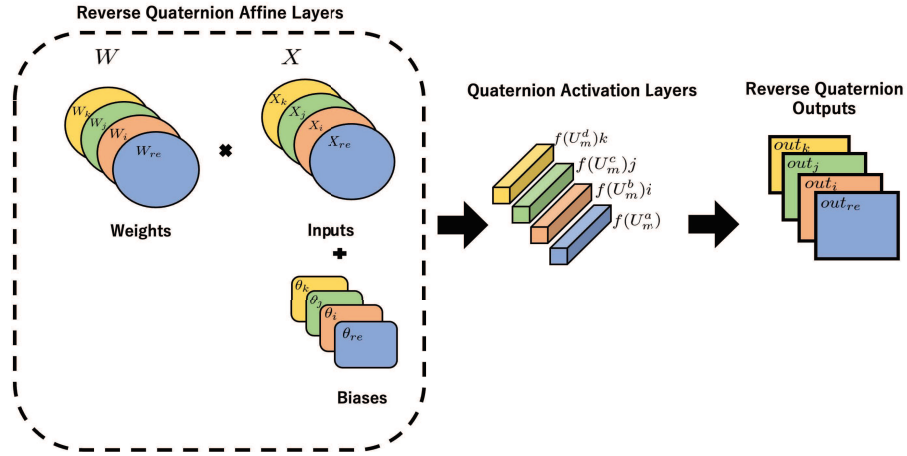


Fig. 1. In the Reverse Quaternion Neural Network, unlike the usual H quaternion neural network, weights are applied in reverse order.

2.3 Reverse Quaternion Neural Network

The multi-layer feedforward reverse quaternion neural network consists of the reverse quaternion neurons described in the previous section.

For the sake of simplicity, consider a three-layer feedforward reverse quaternion neural network. We use $w_{ml} = w_{ml}^a + w_{ml}^b i + w_{ml}^c j + w_{ml}^d k \in \mathbb{H}$ for the weight between the input neuron l and the hidden neuron m , $v_{nm} = v_{nm}^a + v_{nm}^b i + v_{nm}^c j + v_{nm}^d k \in \mathbb{H}$ for the weight between the hidden neuron m and the output neuron n , $\theta_m = \theta_m^a + \theta_m^b i + \theta_m^c j + \theta_m^d k \in \mathbb{H}$ for the bias of the hidden neuron m , $\gamma_n = \gamma_n^a + \gamma_n^b i + \gamma_n^c j + \gamma_n^d k \in \mathbb{H}$ for the bias of the output neuron n . Let $I_l = I_l^a + I_l^b i + I_l^c j + I_l^d k \in \mathbb{H}$ denote the input signal to the input neuron l , and let $H_m = H_m^a + H_m^b i + H_m^c j + H_m^d k \in \mathbb{H}$ and $O_n = O_n^a + O_n^b i + O_n^c j + O_n^d k \in \mathbb{H}$ denote the output signals of the hidden neuron m , and the output neuron n , respectively. Let $\delta_n = \delta_n^a + \delta_n^b i + \delta_n^c j + \delta_n^d k = T_n - O_n \in \mathbb{H}$ denote the error between O_n and the target output signal $T_n = T_n^a + T_n^b i + T_n^c j + T_n^d k \in \mathbb{H}$ of the pattern to be learned for the output neuron n . We define the square error for the pattern p as $E_p = (1/2) \sum_{n=1}^N |\delta_n|^2$, where N is the number of output neurons, and $|x| := \sqrt{x_1^2 + x_2^2 + x_3^2 + x_4^2}$ for $x = x_1 + x_2 i + x_3 j + x_4 k \in \mathbb{H}$.

We used here the same notations as those in [7] for inputs, weights, biases, outputs, errors and target output signals.

2.4 Learning Algorithm

Next, we derive a learning rule for the RQNN described in Section 2.3.

For a sufficiently small learning constant $\varepsilon > 0$, and using a steepest descent method, we can show that the weights and the biases should be modified according to the following equations as in [7]. In this case, the amount of the correction for the RQNN is calculated by obtaining the partial derivatives of the real and imaginary parts separately. This is a variant of the well-known backpropagation learning algorithm using quaternions [16].

$$\begin{aligned} \Delta v_{nm} &:= \Delta v_{nm}^a + \Delta v_{nm}^b i + \Delta v_{nm}^c j + \Delta v_{nm}^d k \\ &= -\varepsilon \left(\frac{\partial E_p}{\partial v_{nm}^a} + \frac{\partial E_p}{\partial v_{nm}^b} i + \frac{\partial E_p}{\partial v_{nm}^c} j + \frac{\partial E_p}{\partial v_{nm}^d} k \right), \end{aligned} \quad (10)$$

$$\begin{aligned} \Delta \gamma_n &:= \Delta \gamma_n^a + \Delta \gamma_n^b i + \Delta \gamma_n^c j + \Delta \gamma_n^d k \\ &= -\varepsilon \left(\frac{\partial E_p}{\partial \gamma_n^a} + \frac{\partial E_p}{\partial \gamma_n^b} i + \frac{\partial E_p}{\partial \gamma_n^c} j + \frac{\partial E_p}{\partial \gamma_n^d} k \right), \end{aligned} \quad (11)$$

$$\begin{aligned} \Delta w_{ml} &:= \Delta w_{ml}^a + \Delta w_{ml}^b i + \Delta w_{ml}^c j + \Delta w_{ml}^d k \\ &= -\varepsilon \left(\frac{\partial E_p}{\partial w_{ml}^a} + \frac{\partial E_p}{\partial w_{ml}^b} i + \frac{\partial E_p}{\partial w_{ml}^c} j + \frac{\partial E_p}{\partial w_{ml}^d} k \right), \end{aligned} \quad (12)$$

$$\begin{aligned} \Delta \theta_m &:= \Delta \theta_m^a + \Delta \theta_m^b i + \Delta \theta_m^c j + \Delta \theta_m^d k \\ &= -\varepsilon \left(\frac{\partial E_p}{\partial \theta_m^a} + \frac{\partial E_p}{\partial \theta_m^b} i + \frac{\partial E_p}{\partial \theta_m^c} j + \frac{\partial E_p}{\partial \theta_m^d} k \right) \end{aligned} \quad (13)$$

where Δx denotes the amount of the correction of a parameter x . The above equations (10) - (13) can be expressed as

$$\Delta v_{nm} = \bar{H} \Delta \gamma_n, \quad (14)$$

$$\begin{aligned} \Delta \gamma_n = \varepsilon & \left((1 - O_n^a) O_n^a \delta_n^a + (1 - O_n^b) O_n^b \delta_n^b \mathbf{i} \right. \\ & \left. + (1 - O_n^c) O_n^c \delta_n^c \mathbf{j} + (1 - O_n^d) O_n^d \delta_n^d \mathbf{k} \right), \end{aligned} \quad (15)$$

$$\Delta w_{ml} = I_l \Delta \bar{\theta}_m, \quad (16)$$

$$\begin{aligned} \Delta \theta_m = (1 - H_m^a) H_m^a \cdot \text{Re} & \left[\sum_n (\Delta \bar{\gamma}_n v_{nm}) \right] \\ & + (1 - H_m^b) H_m^b \cdot \text{Im}^i \left[\sum_n (\Delta \bar{\gamma}_n v_{nm}) \right] \mathbf{i} \\ & + (1 - H_m^c) H_m^c \cdot \text{Im}^j \left[\sum_n (\Delta \bar{\gamma}_n v_{nm}) \right] \mathbf{j} \\ & + (1 - H_m^d) H_m^d \cdot \text{Im}^k \left[\sum_n (\Delta \bar{\gamma}_n v_{nm}) \right] \mathbf{k} \end{aligned} \quad (17)$$

where $\text{Re}[x] := x_1$, $\text{Im}^i[x] := x_2$, $\text{Im}^j[x] := x_3$ and $\text{Im}^k[x] := x_4$ for a quaternion $x = x_1 + x_2 \mathbf{i} + x_3 \mathbf{j} + x_4 \mathbf{k} \in \mathbb{H}$.

For comparison, the amount of the correction for the usual quaternion neural network where xw is calculated for a weight $w \in \mathbb{H}$ and an input signal $x \in \mathbb{H}$ to a quaternion neuron is shown below, which was derived in [7].

$$\Delta v_{nm} = \bar{H}_m \Delta \gamma_n, \quad (18)$$

$$\begin{aligned} \Delta \gamma_n = \varepsilon & \left(\delta_n^a (1 - O_n^a) O_n^a + \delta_n^b (1 - O_n^b) O_n^b \mathbf{i} \right. \\ & \left. + \delta_n^c (1 - O_n^c) O_n^c \mathbf{j} + \delta_n^d (1 - O_n^d) O_n^d \mathbf{k} \right), \end{aligned} \quad (19)$$

$$\Delta w_{ml} = \bar{I}_l \Delta \theta_m, \quad (20)$$

$$\begin{aligned} \Delta \theta_m = (1 - H_m^a) H_m^a \cdot \text{Re} & \left[\sum_n (\Delta \gamma_n \bar{v}_{nm}) \right] \\ & + (1 - H_m^b) H_m^b \cdot \text{Im}^i \left[\sum_n (\Delta \gamma_n \bar{v}_{nm}) \right] \mathbf{i} \\ & + (1 - H_m^c) H_m^c \cdot \text{Im}^j \left[\sum_n (\Delta \gamma_n \bar{v}_{nm}) \right] \mathbf{j} \\ & + (1 - H_m^d) H_m^d \cdot \text{Im}^k \left[\sum_n (\Delta \gamma_n \bar{v}_{nm}) \right] \mathbf{k}. \end{aligned} \quad (21)$$

The meaning of symbols in Eqs. (18) - (21) is the same as those in Eqs. (14) - (17). The differences between the learning rule of the RQNN and the one of the usual quaternion neural network are the positions of $\delta_n^a, \delta_n^b, \delta_n^c, \delta_n^d$ in Eqs. (15) and (19), and the complex conjugate for $\Delta\gamma_n, v_{nm}$ in Eqs. (17) and (21).

3 Experiments

In order to investigate the learning characteristics of the RQNN, we conducted two experiments focusing on learning speed and rotation representation, and evaluated their performance.

We call the multi-layer feedforward quaternion neural network where xw is calculated for a weight $w \in \mathbb{H}$ and an input signal $x \in \mathbb{H}$ to a quaternion neuron *QNN* here for short. Also, we call the multi-layer feedforward real-valued neural network *Real-NN* here for short.

3.1 Learning Speed

First, we compared the learning speeds of the RQNN, the QNN, and the Real-NN. We used the learning data shown in Table 1, which was used in [7].

Table 1. Learning data [7]

Input	Output
$1 + i + j + k$	1
$1 + 2i + j + 2k$	i
$2 + i + 2j + k$	j
$2 + 2i + 2j + 2k$	k

To ensure fairness in computation, the Real-NN was structured as a 4-8-4 fully connected three-layer network, while both the QNN and the RQNN were structured as 1-6-1 fully connected three-layer networks (TABLE 2). Since one quaternion consists of four real numbers, it is calculated as four parameters.

Table 2. Layer configuration for each neural network and the total number of parameters.

Model	Layer	Total Params
Real-NN	4-8-4	76
QNN	1-6-1	76
RQNN	1-6-1	76

The sigmoid function was used for the real-valued function f_R in the activation function (Eq. (9)). The initial first, second, third, and fourth parts of

quaternion weights and quaternion biases were randomly generated from a uniform distribution ranging from -0.3 to 0.3 . The initial real-valued weights and real-valued biases of the Real-NN were also set the same way. The learning rate ε was set to 0.1 . We determined that learning converged when the value of the learning error (loss) was below 0.01 . A total of 100 trials were performed. The average number of iterations required for convergence of 100 trials was evaluated. The results of the experiments are shown in Table 3. The typical learning curves are shown in Fig. 2.

It can be observed from Fig. 2 that despite having higher initial loss values, both the QNN and the RQNN converge more than twice as fast compared to the Real-NN. On the other hand, when comparing the QNN with the RQNN, their learning speeds are almost identical, and their learning curves follow the same trajectory.

Table 3. Average number of iterations required for convergence of 100 trials (Avg \pm Std)

Real-NN	QNN	RQNN
10701.98 \pm 593.71	3111.84 \pm 315.10	3306.22 \pm 681.29

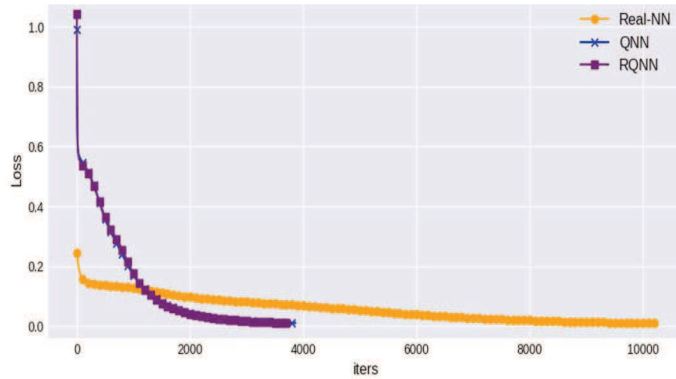


Fig. 2. An example of learning curve. The yellow curve denotes the Real-NN, the blue curve the QNN, and the purple curve the RQNN. The blue and purple lines almost overlap.

3.2 Representation of Rotation

Next, we evaluated the generalization on rotation of the RQNN via a computer simulation: 1) rotation of lines, and 2) rotation of point cloud.

Rotation of lines To investigate the generalization performance on rotation, 200 points were generated at equal intervals along each of the i , j , k axes in 3D space, ensuring that the angle between each data point was 90 degrees (Fig. 3). An experiment was then conducted to examine the behavior of the output of the RQNN for the test data after training. For comparison, the same experiment was also conducted with the traditional QNN. The input learning data were assigned to the points on the i -axis, the teacher data to the points on the j -axis, and the input test data to the points on the k -axis.

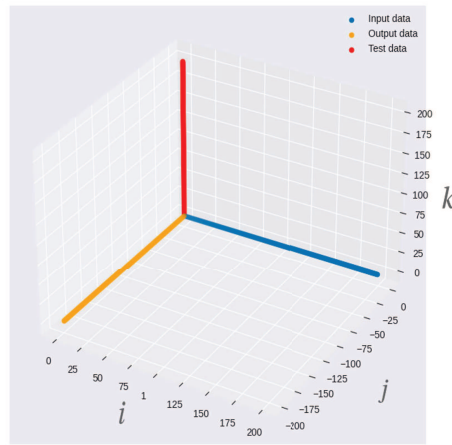


Fig. 3. The blue represents the input learning data, the orange the teacher data, and the green the input test data.

Both the QNN and RQNN were configured as five-layer fully connected neural networks with layer sizes of 4-120-240-120-4. Since the data used in this experiment is linear (Fig. 3), the activation function was set to an identity function. The learning rate was set at 0.05, and training was performed until the training loss value fell below 0.01, with a total of 50 trials. The Adam optimization algorithm was utilized, and weights were initialized using the Xavier uniform distribution. Identical initial values were used for the weights of both the QNN and RQNN.

In order to quantitatively measure the differences in the outputs of the two networks after training, the angles formed by the outputs of both the QNN and the RQNN were calculated using Eq. (22). Additionally, the rotation angles from the input test data to the output data for each point in both the QNN and the

RQNN were computed using the Euler angles (Eqs. (23) - (25)).

$$\cos \theta = \frac{\mathbf{v}_1 \cdot \mathbf{v}_2}{\|\mathbf{v}_1\| \|\mathbf{v}_2\|} \quad \text{where } \mathbf{v}_1, \mathbf{v}_2 \in \mathbb{R}^3, \quad (22)$$

$$\text{roll} = \arctan 2(2(q_w q_x + q_y q_z), 1 - 2(q_x^2 + q_y^2)), \quad (23)$$

$$\text{pitch} = \begin{cases} \arcsin(2(q_w q_y - q_z q_x)), & (\text{if } |2(q_w q_y - q_z q_x)| \leq 1) \\ \frac{\pi}{2} \cdot \text{sign}(2(q_w q_y - q_z q_x)) & (\text{otherwise}), \end{cases} \quad (24)$$

$$\text{yaw} = \arctan 2(2(q_w q_z + q_x q_y), 1 - 2(q_y^2 + q_z^2)) \quad (25)$$

for a quaternion $q = q_w + q_x \mathbf{i} + q_y \mathbf{j} + q_z \mathbf{k} \in \mathbb{H}$. Roll, pitch, and yaw, denoted as roll, pitch, and yaw, respectively, refer to rotations around the x-axis, y-axis, and z-axis. sign is a function that returns the sign of a number.

Fig. 4 displays a visualization of one of the experimental results. The blue line shows the output of the QNN for the input test data (red line) after training, and the purple line shows the output of the RQNN for the same input test data (red line) after training. We can find from Fig. 4 that the QNN and the RQNN output completely different values for the same input test data. Table 4 shows the average and the standard deviation of the angles between the outputs of the QNN and the RQNN, as well as those of the angles between the input test data and the outputs of the QNN over 50 trials, and those of the RQNN. We can find from Table 4 that the QNN and the RQNN learned to rotate about 90 degrees in different ways.

Table 5 shows the Euler angles (Eqs. (23) - (25)) of the rotation from the input test data to the outputs of the QNN and RQNN for the result shown in Fig. 4. It is also obvious from Table 5 that the QNN and the RQNN output completely different values for the same input test data.

Table 4. Average and standard deviation of the angles between the QNN output and the RQNN output over 50 trials

Subject	Avg \pm std
Angle between QNN output and RQNN output	102.5 \pm 48.0
Angle between QNN output and input test data	94.4 \pm 29.9
Angle between RQNN output and input test data	78.9 \pm 39.8

Table 5. Euler angles of rotation from the input test data to the QNN and the RQNN outputs for the result shown in Fig. 4.

	i (roll)	j (pitch)	k (yaw)
Input test data - QNN output	-76.5	14.1	-11.1
Input test data - RQNN output	-23.9	-77.7	19.3

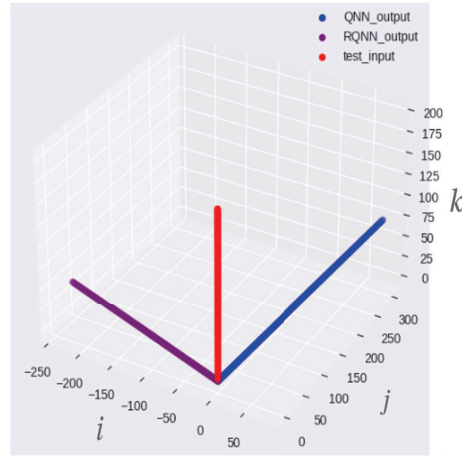


Fig. 4. A visualization of one of the experimental results. The blue line shows the output of the QNN for the input test data (red line) after training. The purple line shows the output of the RQNN for the input test data (red line) after training.

Rotation of point cloud Subsequently, an experiment on rotational representation was conducted using the plane point cloud data shown in the left figure in Fig. 5. These training data consisted of a rectangle composed of 5,000 points on the ij -plane, both vertically and horizontally ranging from 0 to 1, which was used as the input data. The plane rotated 90 degrees around the j -axis was used as the teacher data.

Both the QNN and the RQNN constructed a four-layer fully connected neural network with a 1-25-50-1 architecture. In this experiment as well, since the training data involved linear transformations, an identity function was used as the activation function for all neurons in each layer instead of a nonlinear function. The learning rate was set to 0.05. The Adam optimizer was used, and learning was conducted 10 times until the loss value was less than 0.01. Additionally, the weights were initialized using the Xavier uniform distribution, and the initial values for the RQNN and the QNN were unified.

As the test data, a quadrilateral pyramid consisting of 5,000 points, shown in the right figure of Fig. 5, was used. Fig. 6 visualizes the output values of the QNN and the RQNN for the input test data in one of the ten trials conducted. It can be seen from Fig. 6 that the output of the RQNN is different from the output of the QNN for the same input test data. To quantitatively evaluate the overall motion of this quadrilateral pyramid, we chose the four representative points (red, blue, yellow, and green) characterizing the features of the quadrilateral pyramid, and calculated the Euler angles of rotation of the four vertices of the tetrahedron. Table 6 shows the Euler angles (Eqs. (23) - (25)) of the rotation of the four vertices from the input test data to the outputs of the QNN and RQNN for the result shown in Fig. 6. It is also obvious from Table 6 that the QNN and the RQNN output completely different values for the same input test data.

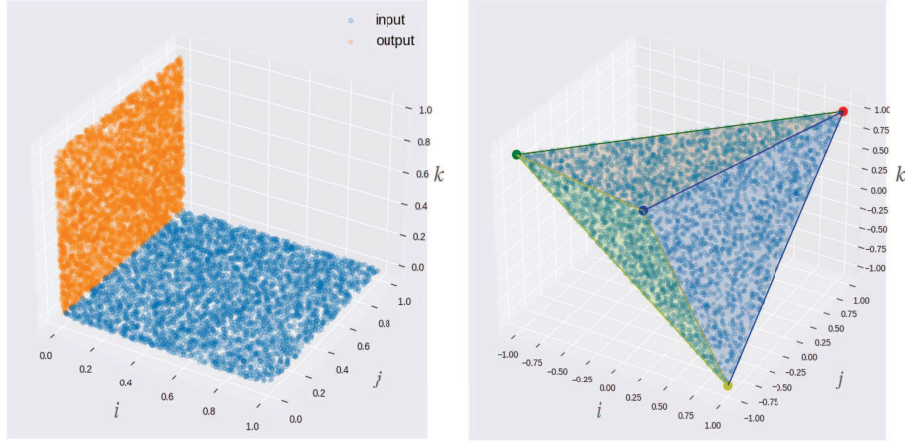


Fig. 5. The left figure shows the training data used in the point cloud rotation experiment. The blue points represent the input data, and the orange points represent the output data. The right figure depicts the test data consisting of 5,000 points forming a quadrilateral pyramid.

For reference, the results of using a nonlinear activation function for the RQNN and QNN in this experiment are shown in Fig. 7 of the appendix. The parameters and training conditions for both models were the same, with the sigmoid function used in the hidden layers and the identity function used in the output layer. As expected, these also produced completely different outputs for the same input test data.

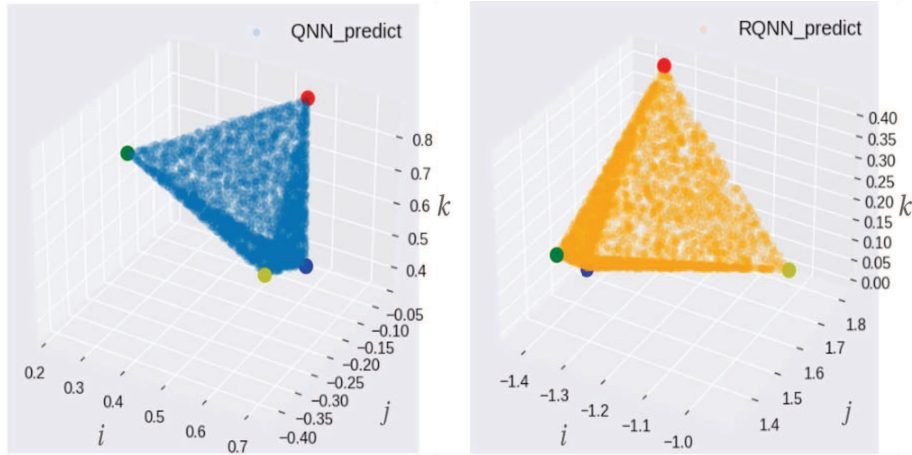


Fig. 6. Outputs of the QNN and the RQNN for the input test data shown in Fig. 5 in the experiment on the point cloud rotation

Table 6. Euler angles of rotation of the four vertices from the input test data to the QNN and the RQNN outputs for the result shown in Fig. 6.

Input test data – QNN output			
	i (roll)	j (pitch)	k (yaw)
Blue	28.4	3.1	-12.1
Red	-5.4	-8.8	14.1
Green	-37.6	13.2	-4.5
Yellow	-15.5	-33.3	48.9

Input test data – RQNN output			
	i (roll)	j (pitch)	k (yaw)
Blue	3.8	1.6	-44.9
Red	-1.0	3.0	-2.1
Green	-38.1	34.6	-12.3
Yellow	-2.8	-18.8	16.5

4 Discussion

The learning speed of the RQNN is several times faster than the Real-NN, but there was no significant difference in learning speed compared to the traditional QNN. As seen in Table 3 and Fig. 2, despite having higher initial losses than the Real-NN, both the QNN and the RQNN converged about three times faster on average. However, between the RQNN and the QNN, the RQNN completed learning in 3,306 epochs, while the QNN took about 3,111 epochs on average, showing no significant difference. This is likely because both the RQNN and the QNN are neural network architectures based on quaternions.

The rotational generalization performance of the RQNN was observed in both the rotation of lines and the rotation of objects generated from point clouds. It is clear from Fig. 4 that there are differences in the output results between the QNN and the RQNN for the input test patterns. Furthermore, as seen in Table 4, the average angle of the outputs between the QNN and the RQNN was 102 degrees, suggesting that the RQNN learned a different rotation than the QNN. The angles between the input test data and the outputs of the QNN and the RQNN are 94.4 and 78.8 degrees on average, respectively, which are similar to the value of angle (i.e., 90 degrees) given during the training. Additionally, examining the rotation angles from the input test data to the QNN and the RQNN using the Euler angles reveals that the outputs of the two models are different (Table 5). Significant differences were observed in rotations around the j-axis, i-axis, and k-axis. Looking at the experimental result on the point cloud shown in Fig. 6, it is apparent that the attitudes of the tetrahedron and the positions of the colored vertices in both the RQNN and the QNN exhibit different behaviors. Furthermore, examining the rotation angles of the colored vertices from the test data using the Euler angles also reveals that the behavior

of the RQNN differs from that of the QNN (Table 6). As a result of conducting two experiments on the generalization performance of rotation, it was discovered that the RQNN acquires a different rotational representation compared to the QNN, despite using models of the same configuration, the same dataset, and the same learning conditions.

5 Conclusion

In this paper, we proposed a new multi-layer feedforward quaternion neural network model architecture, the Reverse Quaternion Neural Network, utilizing the non-commutative nature of quaternion multiplication, and investigated its learning characteristics. Comparing the results of the experiments on convergence speed and the rotational generalization performance with the traditional models, it was found that the learning speed of the Reverse Quaternion Neural Network is similar to that of the conventional quaternion neural network, but the Reverse Quaternion Neural Network has a different generalization on rotation.

As a future challenge, it is important to further investigate the learning representation characteristics of the RQNN. In this paper, relatively simple experiments were conducted, and differences in behavior were identified, but it is necessary to explore the potential of the RQNN through experiments using more complex learning datasets. Moreover, regarding the generalization performance on rotation, it is also necessary to investigate from a theoretical perspective. By mathematical analyses, it would be clarified in which areas the RQNN has advantages compared to traditional models.

6 Appendix

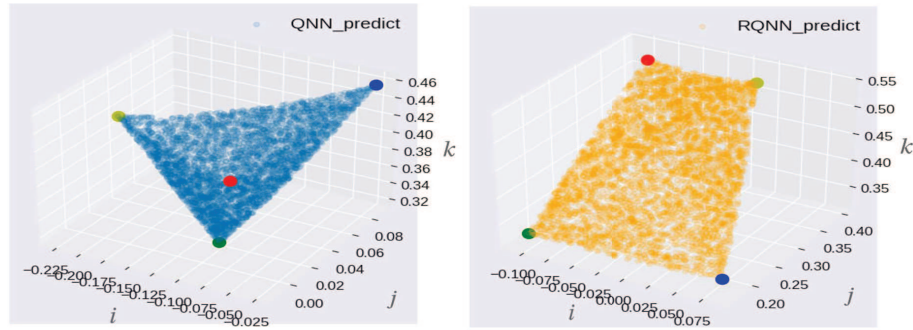


Fig. 7. Outputs of the QNN and the RQNN using the sigmoid function in the hidden layers and the identity function in the output layer in the point cloud rotation experiment for the input test data shown in Fig. 5

References

1. Hirose, A.: Complex-Valued Neural Networks: Advances and Applications. IEEE Press/Wiley (2013)
2. Lee, C., Hasegawa, H., Gao, S.: Complex-valued neural networks: A comprehensive survey. *IEEE/CAA Journal of Automata Sinica* **9**(8), 1–21 (2022)
3. Goh, V.S.L., Mandic, D.P.: Complex Valued Nonlinear Adaptive Filters: Noncircularity, Widely Linear and Neural Models. Wiley, New York (2009)
4. Nitta, T.: Complex-Valued Neural Networks: Utilizing High-Dimensional Parameters. Information Science Reference, Pennsylvania, USA (2009)
5. Parcollet, T., Morchid, M., Linares, G.: A survey of quaternion neural networks. *Artificial Intelligence Review* **53**, 2957–2982 (2020). Springer, <https://doi.org/10.1007/s10462-019-09752-1>
6. Nitta, T.: An Extension of the Back-Propagation Algorithm to Complex Numbers. *Neural Networks* **10**, 1391–1415 (1997)
7. Nitta, T.: A quaternary version of the back-propagation algorithm. In: Proceedings of ICNN'95 - International Conference on Neural Networks, vol. 5, pp. 2753–2756 vol.5 (1995). <https://doi.org/10.1109/ICNN.1995.488166>
8. Nitta, T., Furuya, T.: A complex back-propagation learning. *Transactions of Information Processing Society of Japan* **32**(10), 1319–1329 (1991). In Japanese
9. Nitta, T.: A complex numbered version of the back-propagation algorithm. In: Proc. INNS World Congress on Neural Networks (WCNN1993), vol. 3, pp. 576–579 (1993), Portland, July 11–15
10. Zhu, X., Xu, Y., Xu, H., Chen, C.: Quaternion Convolutional Neural Networks. In: Proceedings of the European Conference on Computer Vision (ECCV), September (2018)
11. LeCun, Y., Bottou, L., Bengio, Y., Haffner, P.: Gradient-based learning applied to document recognition. *Proceedings of the IEEE* **86**(11), 2278–2324 (1998)
12. Parcollet, T., Zhang, Y., Morchid, M., Trabelsi, C., Linares, G., De Mori, R., Bengio, Y.: Quaternion Convolutional Neural Networks for End-to-End Automatic Speech Recognition. In: Proc. Interspeech 2018, pp. 22–26 (2018). <https://doi.org/10.21437/Interspeech.2018-1898>
13. Hamilton, W.R.: ON QUATERNIONS, OR ON A NEW SYSTEM OF IMAGINARIES IN ALGEBRA By William Rowan Hamilton, <https://www.maths.tcd.ie/pub/HistMath/People/Hamilton/OnQuat/OnQuat.pdf>, last accessed 2023/10/25
14. Matsui, N., Isokawa, T., Kusamichi, H., Peper, F., Nishimura, H.: Quaternion neural network with geometrical operators. *Journal of Intelligent & Fuzzy Systems* **15**(3–4), 149–164 (2004)
15. Yoshida, M., Kuroe, Y., Mori, T.: Models of Hopfield-type quaternion neural networks and their energy functions. *International journal of neural systems* **15**, 129–135 (2005)
16. Rumelhart, D.E., Hinton, G.E., Williams, R.J.: Learning internal representations by error propagation. In: *Parallel Distributed Processing: Explorations in the Microstructures of Cognition*, vol. 1, pp. 318–362. MIT Press, Cambridge, MA (1986)